Materials Chemistry and Physics 275 (2022) 125197

Contents lists available at ScienceDirect

Materials Chemistry and Physics

journal homepage: www.elsevier.com/locate/matchemphys

Effect of coal fly ash treatments on synthesis of high-quality zeolite A as a potential additive for warm mix asphalt

Bruno C. Amoni [a], Armando D.L. Freitas [a], Raquel A. Bessa [a], Cristiane P. Oliveira [a], Moisés Bastos-Neto [b], Diana C.S. Azevedo [b], Sebastiao M.P. Lucena [b], José M. Sasaki [c], Jorge B. Soares [d], Sandra A. Soares [a], Adonay R. Loiola [a,*]

[a] Department of Organic and Inorganic Chemistry, Federal University of Ceará, Campus do Pici, 60440-900, Fortaleza, CE, Brazil
[b] Department of Chemical Engineering, Federal University of Ceará, Campus do Pici, 60440-900, Fortaleza, CE, Brazil
[c] Department of Physics, Federal University of Cearv, Campus do Pici, 60440-900, Fortaleza, CE, Brazil
[d] Department of Transportation Engineering, Federal University of Ceará, Campus do Pici, 60440-900, Fortaleza, CE, Brazil

HIGHLIGHTS

- High-quality zeolite A is successfully obtained from fly ash.
- Fly ash is subjected to different treatments prior to zeolite syntheses.
- A novel pore characterization method based on CO_2 isotherms and molecular simulation is applied.
- The obtained zeolite acts decreasing the work temperature of mix asphalt.

GRAPHICAL ABSTRACT

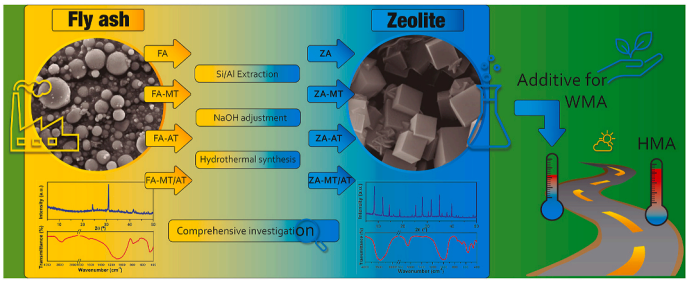

ARTICLE INFO

Keywords:
Zeolite A
Microporous material
Fly ash
Warm mix asphalt
Industrial waste

ABSTRACT

An experimental investigation on the synthesis of zeolite A, based on the treatment of fly ash and controlled extraction of silica and alumina from coal fly ash, combined with the adjustment of the reaction mixtures aiming minimum amount of secondary phases, is presented herein. The precursor samples of fly ash and the obtained zeolites were widely characterized considering different techniques including powder X-ray diffraction, infrared vibrational spectroscopy, scanning electron microscopy, and thermogravimetric analysis. A new pore characterization technique that combines experimental CO_2 isotherms at 273 K and molecular simulation was specially developed for this system. The synthesized zeolites presented zeolite A as the major phase, with high crystallinity and low degree of defects in the supercages. The treated fly ashes affected the synthesis yield and the properties of the obtained zeolites, which proved to be efficient in decreasing the viscosity of the modified asphalt cement, during heating, contributing to improve its workability.

* Corresponding author.
E-mail address: adonay@ufc.br (A.R. Loiola).

https://doi.org/10.1016/j.matchemphys.2021.125197
Received 25 May 2021; Received in revised form 23 July 2021; Accepted 2 September 2021
Available online 2 September 2021

1. Introduction

Coal is the world's most abundant fossil fuel, with reserves of approximately one trillion tons [1], making coal combustion an important process for generating electricity in many countries [2]. When burned in thermal power plants, it generates residues in form of tiny particles which are carried by the combustion gases. Such residues are called fly ashes and are collected by filter systems. Fly ashes are thin particles in powder form, with a predominately spherical shape, either compact or hollow, with maximum diameter of 75 μm and blackish coloration which varies depending on its composition. Their chemical composition is mainly silica (SiO_2), alumina (Al_2O_3), iron oxide (Fe_2O_3), and calcium oxide (CaO) [3]. The dominant mineral phases that compose fly ashes are quartz, kaolinite and ilite, while less predominant phases such as calcite, pyrite and hematite can also be found [4]. Fly ashes are classified into two groups, depending on the combination of SiO_2, Al_2O_3, and Fe_2O_3. Fly ash containing more than 70% of these three compounds is classified as F type, while a concentration in the range 50–70% implicates in a fly ash type C, in which concentration of CaO tends to be higher [5,6].

As a solid residue, fly ash is discarded in open pit deposits and, given its ease of leaching by water, metals such as cadmium, cobalt, chromium, nickel, and lead can be released, strongly impacting the environment [7,8]. Therefore, fly ash accumulation represents a serious environmental problem which needs thorough consideration. In fact, there are numerous studies demonstrating its potential for other purposes [9], including the synthesis of zeolites [10,11].

Zeolites comprise a class of porous aluminosilicates with crystalline structure. Their structure can be summarized as a combination of tetrahedral $[SiO_4]^{4-}$ and $[AlO_4]^{5-}$ joined by oxygen atoms [12]. Their chemical composition is commonly represented by:

$$A_{y/m}^{m+}\left[(SiO_2)_x\left(AlO_2^{2-}\right)_y\right]\cdot zH_2O$$

where A is a cation with charge m, (x + y) is the number of tetrahedra per crystallographic unit cell, and x:y is the silicon:aluminum ratio that, based on the Löwenstein's rule, cannot be higher than 1, and therefore the Al–O–Al linkages are not allowed [13].

Properties as high ion exchange capacity, high surface area, and high chemical stability, make zeolites suitable materials to be employed in innumerous applications such as adsorption in gas purification, ion exchanger in builders, catalysis in oil refining, petrochemistry and biotechnology [14]. Zeolites can be synthesized via many different routes and from different sources. The hydrothermal method is the most common route and involves the treatment of the reagents in strong alkaline medium, together with heating in a closed system. In some cases, ultrasound and microwave radiation can be used as more effective energy sources [15,16]. The raw materials used include silica and aluminum sources such as sodium aluminate and silicate salts, colloidal silica, aerosol silica, as well as other materials as clays [17] and fly ash [18,19]. In fact, the first investigations of zeolite synthesis from fly ash were based on its similarity with volcanic material, a precursor of natural zeolite [20,21].

Nevertheless, synthesizing zeolites from fly ash is not a straightforward task, since high temperatures (90–225 °C) and prolonged synthesis times (24–72 h) are required [22]. Two activation methods are usually applied. In the first one, alkaline fusion takes place at high temperatures, followed by hydrothermal treatment. The second method is the direct hydrothermal, in which the fusion step is omitted. In any case, obtaining the zeolite involves a series of variables such as the type and concentration of the alkali solution used, solution/solid ratio, aging time, mixture techniques, pressure during crystallization, and heating sources [23]. Several works report the synthesis of zeolites as mixtures of phases, as zeolites X, P, Q and S [24], A and T [25]. Musyoka et al. reported the synthesis of zeolite A [26] and X [27] by means of fly ash alkali fusion at 550 °C, followed either by hydrothermal reaction under autogenous pressure in closed system or by reaction using ultrasound. A combination of methods resulted in synthesis of zeolites A and P by activating ashes with concentrated sodium hydroxide solution and adjusting the silicon/aluminum ratio by dissolving metallic aluminum [28]. The main difficulties faced in zeolite synthesis from fly ash are related to the crystallization of secondary phases.

Within their pore structures, zeolites retain considerable amounts of water, which can be released by heating. Zeolite type A in particular can retain approximately 20 wt% of water, being therefore a potential additive in the preparation of warm mix asphalt (WMA). Water-containing technologies promotes the micro-foaming of the asphalt binder, which causes a better coating of the aggregate at lower temperatures than conventional ones [29]. As a consequence of water being released from zeolite, a typical zeolite/WMA can be manufactured at temperatures 20–40 °C lower than an equivalent hot mix asphalt (HMA). Additionally, warm mixtures are presented as an alternative to reduce the emission of CO_2 and polluting gases, as well as to reduce energy consumption, contributing to minimize environmental impacts associated to asphalt preparation. In this context, and considering the complexity in using fly ash for zeolite synthesis, this study investigates the synthesis of zeolite type A from fly ash and its potential as a cost-effective additive for WMA.

2. Experimental

2.1. Materials

Fly ash (FA) used in this work was provided by the ENEVA-Pecém thermal power plant located at Ceará, Brazil. The ashes were collected from the manga filters and are classified as fly ash class F [30]. Prior to the treatments the FA was ground and sieved (<74 μm**).** The base Asphalt Cement (AC) with penetration grade 50/70 was provided by Lubnor (Petrobras, Brazil). Table 1 presents the datasheet related to the main properties obtained from the empirical and rotational viscosity tests. Additional information about AC and zeolite modified AC is presented in Table S1.

2.2. FA treatments

FA was submitted to three different treatments. The first one consisted of the removal of the magnetic fraction by spreading FA samples between two thin paper sheets and applying Neodymium-based magnet on the paper surface in smooth movements repeated times. The remaining non-magnetic fraction was referred as FA-MT (fly ash-magnetic treated). For the acid treatment, 10.00 g of FA were mixed with 100 mL of HCl 2.0 mol L^{-1} and heated at 90 °C for 1 h, under reflux and vigorous magnetic stirring. The remaining solid was washed with deionized water 3 times, dried at 80 °C overnight, and named as FA-AT (acid treated samples). Finally, the last treatment consisted of a combination of magnetic separation and acid treatment (FA-MT/AT).

2.3. Zeolite synthesis

For the zeolite synthesis, 10.0 g of each sample, i.e., the untreated one (FA) and those submitted to different treatments (FA-MT, FA-AT and

Table 1
Asphat cement data for the empirical and rotational viscosity tests.

Assays	Standards	Results
Empirical tests		
Penetration at 25 °C (dmm)	ASTM D5	58
Softening point (°C)	ASTM D36	48
Brookfield viscosity tests		
135 °C (cP)	ASTM D 4402	394.2
150 °C (cP)	ASTM D 4402	191.7
177 °C (cP)	ASTM D 4402	70.0

Source: Asphalt cement datasheet.

FA-MT/AT), were added to 100 mL of NaOH 4.00 mol L^{-1}, in a polypropylene flask coupled to a reflux apparatus, and heated to 90 °C under vigorous magnetic stirring for 1 h. The amount of silica and alumina extracted to the solution was determined indirectly by means of X-ray fluorescence analyses of the solid residues. The zeolite syntheses were carried out via hydrothermal route using the NaOH-extracted silica and alumina from the samples FA, FA-MT, FA-AT and FA-MT/AT, as the only silica source and the main aluminum source. In all cases, the following reactional mixture was used:

3.165 Na_2O : Al_2O_3 : 1.926 SiO_2 : 128 H_2O

As the treatments employed affected the amount of aluminum in the fly ash NaOH-extracted solution, the composition of the reaction mixtures was adjusted by using sodium aluminate. NaOH also had to be added to the reaction mixture so that the required concentration could be achieved. Nevertheless, it was observed that part of the iron present in the fly ashes samples precipitates in form of iron hydroxide during the silica and alumina extraction process. This way, the correspondent decreasing in the NaOH concentration had to be balanced, which was accomplished considering the amount of iron present in the solid residues obtained from the alkali extraction.

The precursor synthesis gels were transferred to a Teflon-lined stainless-steel autoclave and heated at 100 °C for 4 h under autogenous pressure and static conditions. The obtained solid was washed several times with distilled water until constant pH and dried at 80 °C overnight. The zeolites obtained from the different FA samples were named: ZA, ZA-AT, ZA-MT, and ZA-MT/AT.

2.4. Characterization

The efficiency of the zeolite synthesis from fly ash is a requirement for a proper assessment of the zeolite effect as an additive for WMA. Therefore, a comprehensive structural, spectroscopic, and morphological study of the synthesized zeolites was carried out. The characterization of precursor samples as well as the synthesized zeolites was conducted by means of X-ray diffractometry, infrared spectroscopy, scanning electron microscopy and cation exchange capacity determination. In molecular sieves with very small access windows such as zeolite A, clinoptilolite and chabazite, the use of either N_2 or Ar for obtaining adsorption/desorption isotherms at low temperatures is not feasible. For this reason, herein we apply a new approach to characterize the pore volume combining data from experimental CO_2 adsorption isotherms at 273 K with molecular simulation.

2.4.1. X-ray diffraction (XRD)

Powder XRD patterns for the samples with particle sizes below 74 mm (400 mesh) were collected using a X-ray powder diffractometer Xpert MPD (Panalytical). The X-ray tube (Co) operated at 40 kV and 40 mA. The high-resolution diffraction is obtained with a hybrid monochromator for incidence beam, which consists of mirror and Ge monochromator producing a parallel and highly monochromatic beam, respectively. The data were collected with Pixcel solid-state detector. The XRD measurements were performed by using a 255 channels detector, with step scan of 0.013° in 2θ angular interval from 5° to 50°.

Structure refinement was performed for the resulting zeolite samples by Rietveld method using GSAS software package with EXPGUI interface [31,32], observing the adjustments between observed and calculated patterns by the χ^2 parameter. From these results, quantitative analysis was carried out and average crystallite sizes were calculated by means of Scherrer equation [33] using the full-width at half maximum (FWHM) of the diffraction peaks, which was corrected for instrumental broadening (measured through analysis of LaB_6 crystals, SRM 660C).

2.4.2. Infrared vibrational spectroscopy

Fourier transform infrared (FTIR) spectra were obtained for samples prepared in KBr wafers using a Shimadzu IRTracer-100 FTIR spectrometer in the region 4000-400 cm^{-1} and nominal resolution of 2 cm^{-1}.

2.4.3. Scanning electron microscopy (SEM)

A FEG equipment model Quanta 450 was used with detectors for secondary electrons and energy-dispersive X-ray. Prior to the analyses, samples were prepared on an aluminum support using carbon double-sided sticky tape and coated with a thin gold layer.

2.4.4. Cation exchange capacity (CEC)

CEC of all samples were determined by promoting cation exchange with ammonium ion. In short, 1.00 g of each sample was added to 10.0 mL of NH_4^+ 10 wt%, stirred in orbital shake for 8 h, followed by 16 h in static conditions. The solids were collected, washed several times with distilled water, and dried at 60 °C overnight. The quantification of NH_4^+ ions was carried out by thermal decomposition of ammonium to ammonia, which was titrated with H_2SO_4 0.01 mol L^{-1}. The results were converted to mol kg^{-1}.

2.4.5. Thermal analysis

Thermal analysis of ZA sample was performed using equipment Netzsch model STA 499 F3 in a temperature range of 25–350 °C with heating rate of 5 °C min^{-1} and under nitrogen atmosphere with flow of 50 mL min^{-1}. DCS analysis was carried out in equipment Shimadzu DCS-50, in a temperature range of 25–350 °C with heating rate of 5 °C min^{-1}.

2.4.6. CO_2 adsorption/desorption isotherms and molecular simulation

CO_2 adsorption isotherms were obtained at 273 K in an Autosorb-iQ$_3$ equipment (Quantachrome, USA) and used to characterize the micropore volume of the studied zeolites. The samples (*ca.* 0.1 g) were previously degassed under the following conditions: heating under high vacuum (10^{-4} mbar), from room temperature to 180 °C, at a heating rate of 2 °C min^{-1}, maintaining at the final temperature for a period of 6 h.

Molecular simulation was used to determine the pore integrity of the synthesized zeolite samples. A new approach involving the use of local isotherms of a limited number of zeolite supercages/unit cell was applied. The zeolite A model (Si/Al ratio = 1) used, was obtained through the crystal refinement performed by Pluth and Smith [34]. The model consists of 64 atoms at site I, 24 atoms at site II and 8 atoms at site III, resulting in a unit cell of $Na_{96}Si_{96}Al_{96}O_{384}$. The CO_2 model was taken from Harris and Yung study [35], which fully reproduces the liquid-vapor equilibrium. The system can be properly described by using Lennard-Jones potentials plus Coulomb contributions. Monte Carlo simulation in the grand canonical ensemble was performed to evaluate adsorption isotherms using the force field adapted from the study of Gomes et al. [36].

2.5. Mixing and procedures of asphalt cement (AC) modification with zeolite

The sample ZA was chosen for modification of asphalt cement. Although the yield for the sample ZA was found slightly lower than that of the other synthesized zeolites, its adsorption capacity, measured by CO_2 isotherms at 273 K, was the highest, being 10–18% higher compared to the samples ZA-AT, ZA-MT, and ZA-MT/AT. Besides that, its production involves the simplest route, and therefore it is the most cost-effective material. Thus, this sample was chosen for modification of asphalt cement. In a typical procedure, 4.00 g of zeolite ZA was slowly added to 400.00 g of AC, under mechanical stirring (1500 rpm) at 90 ± 5 °C, for 2 h, using mixer IKA, model RW20. The additive content was 1 wt% of the binder, which was chosen based on previous studies [37,38].

2.6. The effect of WMA zeolite additive on asphalt cement properties

In this study, different parameters were considered to evaluate the effect of zeolite as additive for WMA technology: a) to verify the water

release from zeolite, a temperature of 90 °C was used [39,40], b) to investigate the AC viscosity over time, either with or without the synthetized zeolite, the temperature was 120 °C, which is normally used to test the viscosity over time for warm mix asphalt, typically 10–20 °C lower than conventional hot mix asphalt (HMA) [41].

2.6.1. Rotational viscosity test to evaluate asphalt cement foaming through zeolite addition

The rotational viscosity was determined for both AC and zeolite modified AC (ZA-AC), using a viscosimeter Brookfield model DVII+. The tests were performed at constant temperature (120 °C) and the viscosity values were determined over time. The first two values were recorded at 0.5 and 1 min, respectively, and the subsequent ones at intervals of 5 min, to a total of 31 min.

3. Results and discussion

In this section, a comprehensive characterization of the fly ash samples, and the synthesized zeolites is presented. A set of different techniques was employed to assess the effectiveness of the synthesis and the potential of the obtained materials for application in warm mix asphalt.

3.1. XRD

Fig. 1a–d shows the powder XRD patterns for the samples of fly ash and the treated fly ash samples. All samples present quartz, hematite, and magnetite as the major components. Mullite appears only in the untreated fly ash sample (Fig. 1a).

The XRD patterns of the synthesized zeolites are presented in Fig. 1e–h. The main results for the Rietveld structural refinement are

Table 2
Rietveld refinement output. The major phases are indicated in bold.

Sample	Phase	Weight/ %	χ^2	Average crystallite size/nm
ZA-MT/ AT	**Zeolite A (24901)**	**100**	1.01	102.4
ZA-MT	**Zeolite A (24901)**	**100**	1.02	133.8
ZA-AT	**Zeolite A (24901)**	**95.5**	1.14	77.1
	Zeolite Y (201472)	1.8		14.7
	Zeolite RUB-3 (86547)	0.6		75.0
	Quartz (26430)	2.1		217.0
ZA	**Zeolite A (24901)**	**96.4**	0.93	87.3
	Zeolite ZK-14 (201587)	3.6		42.5

ICSD-Inorganic Crystal Structure Database.

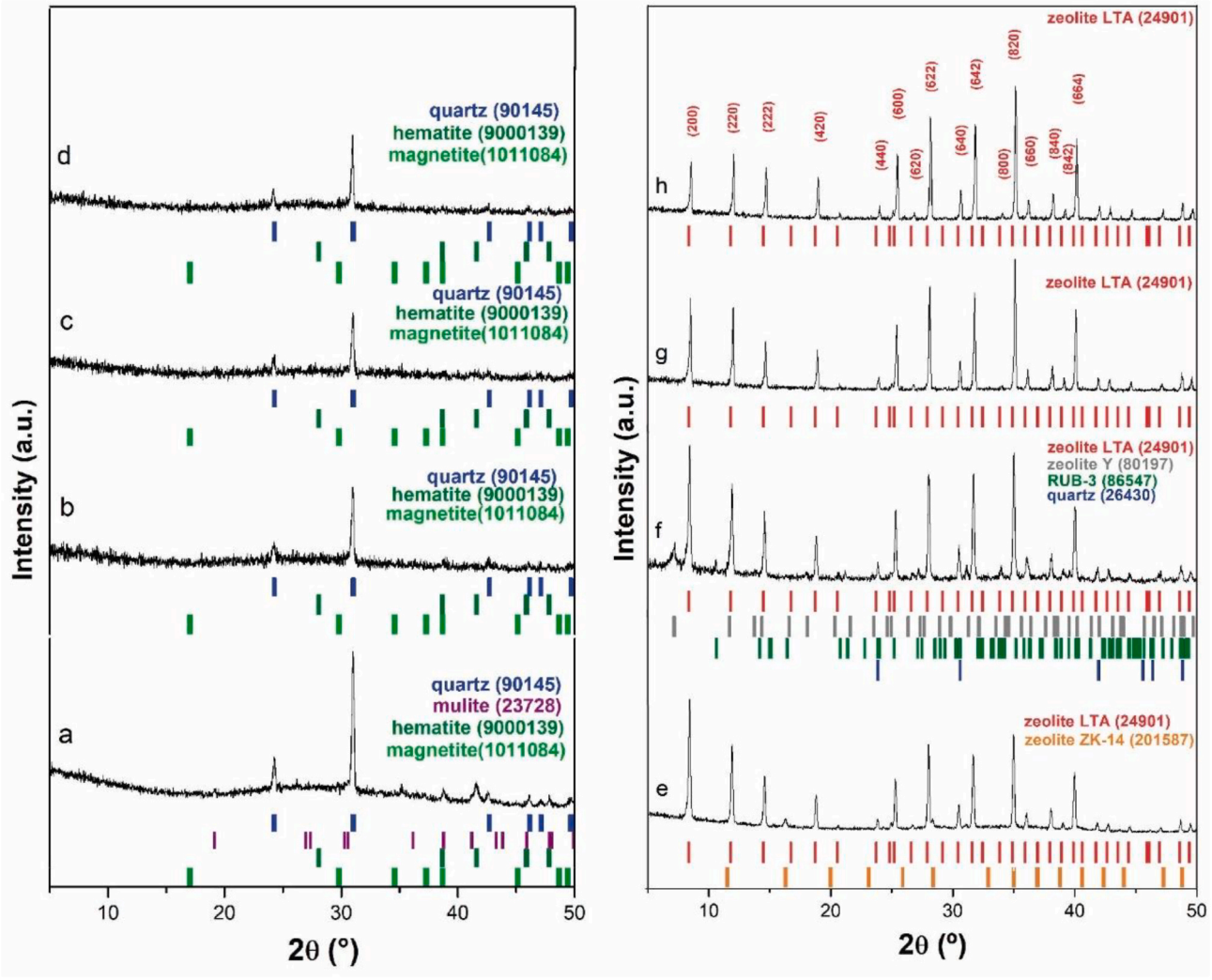

Fig. 1. XRD patterns of fly-ash (a) without treatment (FA), and with treatment (b) FA-MT, (c) FA-AT, and (d) FA-MT/AT; XRD patterns of synthesized zeolites (e) ZA, (f) ZA-AT, (g) ZA-MT, and (h) ZA-MT/AT.

summarized in Table 2 and in Fig. S1. The closer the value of χ^2 to 1.0, the better the adjustment. The results of χ^2 showed in Table 2 indicate, therefore, that the refinement is reliable.

In all the synthesized zeolite samples (Fig. 1e–h), zeolite A (ICSD 24901) [42] is found as the major crystalline phase, with the correspondent peaks well defined and presenting high intensity. Samples ZA (Fig. 1e) and ZA-AT (Fig. 1f) presented secondary phases in small amounts, while the samples ZA-MT (Fig. 1g) and ZA-MT/AT (Fig. 1h), obtained from the fly ash samples subjected to magnetic separation and to the combination of magnetic separation with acid treatment, respectively, were composed of pure zeolite A phase. The absence of secondary phases in the synthesized samples lead to bigger zeolite crystallite, indicating that in an environment without competition, the zeolite tends to grow more easily. The sample ZA-MT/AT (Fig. 2h) presents peaks at 8.55° 2θ (200) and 12.04° 2θ (220) with relative intensity opposite to what is observed in the other samples. This is commonly associated to preferred orientation and may be related to the distribution of occupancy of specific T-sites by Al or even Fe atoms. The acid treatment of the fly ash promotes the removal of iron, what would potentially affect the zeolite crystallization. However, this treatment also removes aluminum from the fly ash, affecting the Si/Al ratios of the reactional mixtures and consequently the Si/Al ratio in the zeolites, which is a well-known parameter that strongly influences the chemical functionality of zeolites [43].

3.2. Chemical composition and cation exchange capacity

The amount of Si, Al, and Fe, as well as CEC values, for all the samples, are shown in Table 3. For comparison purposes, a sample of zeolite A (A) synthesized via the classical method, employing sodium metasilicate and sodium aluminate, is also included. It is possible to observe that the Si/Al ratio varies depending on the treatment applied to the ashes. The CEC values determined for the zeolite samples varied from 1.53 to 2.26 mol kg^{-1}, which are considerably higher than the values verified for the precursor samples and slightly higher than that observed for the reference zeolite (sample A). These numbers are compatible with results from other works [44–46]. Furthermore, it is also important to highlight that the sample ZA-MT/AT showed the highest CEC value, reinforcing the effectiveness of the fly ash combined treatment for the synthesis of zeolite with improved properties.

Table 3
Chemical composition, determined by EDS, and cation exchange capacity (CEC), determined by Kjeldahl method, of the fly ash and the synthesized zeolite samples.

Sample	Si/%	Al/%	Fe/%	Si/Al	CEC/mol kg^{-1}
A	19.9	17.9	0.0	1.069	1.267
FA	27.18	14.25	6.46	1.831	0.1461
ZA	18.66	18.89	0.82	0.947	2.142
FA-MT	32.97	15.52	10.22	2.038	0.1614
ZA-MT	22.10	21.34	0.25	0.995	1.535
FA-AT	34.42	10.94	4.13	3.027	0.3332
ZA-AT	23.37	21.43	0.0	1.061	1.665
FA-MT/AT	34.13	11.38	6.09	2.886	0.1952
ZA-MT/AT	19.97	20.32	0.0	0.944	2.261

3.3. FTIR

As vibrational spectroscopy in the infrared region provides important information related to specific chemical bonds, it is helpful for evaluating the influence of the treatments applied to the fly ashes and the structural changes associated to the synthesized zeolites. FTIR spectra of the fly ash samples are presented in Fig. 2a–d. Three main signals are observed: the large band centered at 1085 cm^{-1}, which can be associated with the presence of aluminosilicates with some amorphous nature, the band at 470 cm^{-1} related to O–Si–O bending vibrations, and the band at 788 cm^{-1}, characteristic of O–Si–O symmetric stretching vibration [47]. No substantial changes were observed for the fly ash samples after the treatments (Fig. 2b–d), except for some slightly improvement in the resolution of the large band at 1085 cm^{-1} for the samples FA-MT and FA-MT/AT, what can be associated to elimination of Fe-rich particles present in the FA.

The spectra of the synthesized zeolites are shown in Fig. 2e–h. Compared to the fly ash samples spectra (Fig. 2a–d), several new bands can be observed, clearly indicating tranformation of their structures. The region between 700 and 400 cm^{-1} is known as the fingerprint zone, due to specific vibrational modes related to the zeolite structure. For the synthesized zeolites, it is possible to observe three bands in this region. The band centered at 462 cm^{-1} is characteristic of internal vibration of Si (Al)–O bending, while the band at 557 cm^{-1} is due internal vibration of double-four rings. The strong signal at 1002 cm^{-1} can be associated to Si (Al)–O asymmetric stretching [48,49]. The large band at 3450 cm^{-1} and the well defined band at 1648 cm^{-1} are related to the presence of structural water in the zeolites.

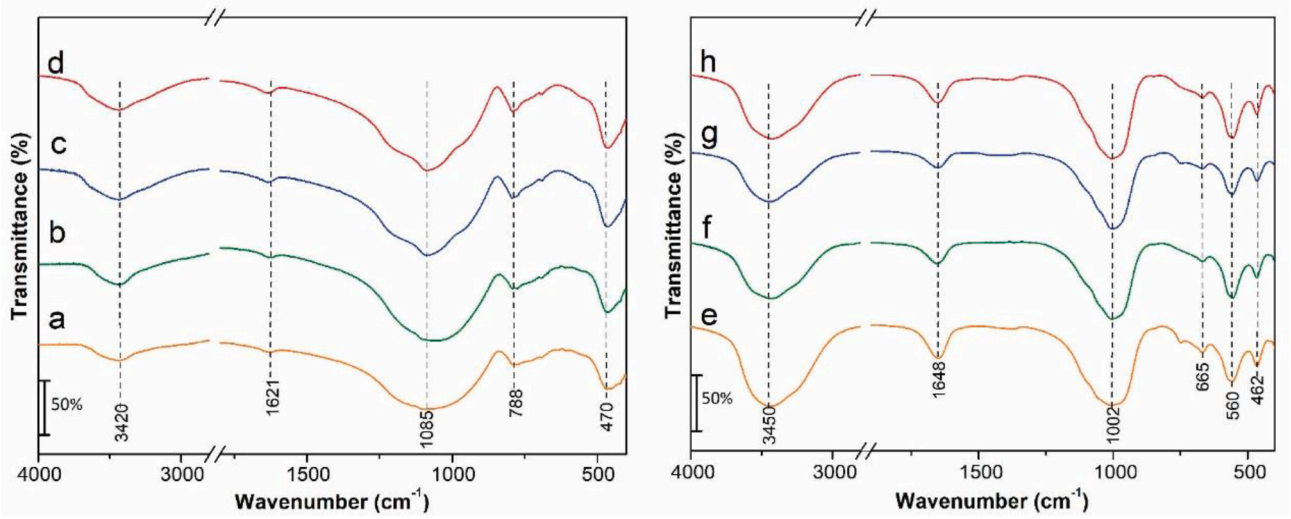

Fig. 2. FTIR spectra of fly-ash samples: (a) with no treatment, (b) with acid treatment, (c) with magnetic treatment. and (d) with combined magnetic and acid treatments; FTIR spectra of synthesized zeolites (e) ZA, (f) ZA-AT, (g) ZA-MT, and (h) ZA-MT/AT.

3.4. SEM

SEM is a valuable technique for morphology and surface texture studies of the individual particles. The SEM images for the fly ash samples, presented in Fig. 3, show uniform spherical particles, supposedly hollow, commonly referred to as cenospheres. These particles are formed during the expansion of the gases produced in the burning of the coal. It is possible to visualize a smoothing over the particle surfaces after the acid treatment (Fig. 3c–d and g-h), what might be the result of the acid attack to the iron oxides compounds deposited on these particles [50,51].

Particle morphology is usually an important factor for the final properties of several materials. Surface features of zeolite A may vary substantially [52,53], and as the zeolite morphology affects directly its applications [54], it is crucial to understand how the treatments applied to the fly ash samples affects the morphology of the synthesized zeolites. SEM images of the synthesized zeolites are presented in Fig. 4.

In all the samples, the characteristic cubic crystal of zeolite A is observed, with apparent homogeneous size distribution. Sample ZA (Fig. 4a and b) shows well-defined sharp edges, while all the other samples present chamfered edges (Fig. 4c–h). This difference in the crystal habits may be associated with many variables. Nevertheless, the reaction mixture composition is believed to be the major responsible for changes in the crystal morphologies. Results from early studies have indicated that the nature of the aluminum source plays a central role in zeolite A morphology [55]. In general, its organic form favors zeolite crystals with chamfered edges, possibly by influencing the water activity in the gel synthesis. As shown in Table 3, the FA sample possesses 14.25 wt% of aluminum, but its concentration is reduced to 10.94 wt% and 11.38 wt% with acid treatment, in sample FA-AT, and with the combined magnetic/acid treatment, respectively.

3.5. CO_2 adsorption/desorption and molecular simulation

N_2 (at 77 K) and Ar (at 87 K) are the most accepted molecules used as probes for textural characterization of porous materials. However, due to a pronounced molecular sieved effect accompanied by packing limitations, at low temperatures the rate of diffusion of N_2 and Ar into the microporous system of zeolite A is extremely slow, particularly in the sodic form of this zeolite, which limits the physisorption capacity for these gases [56].

Some studies suggest the use of CO_2 isotherms at 273 K as an alternative strategy for the characterization of materials in which the pores are inaccessible to N_2 and Ar, at cryogenic temperatures [57]. However, due to the strong CO_2–CO_2 interaction and the lack of a proper theoretical background, characterization methods such as BET, BJH and phenomenological approaches based on CO_2 isotherms can be misleading. Furthermore, even the most recent commercial analyzers provide no kernels that allow the application of NLDFT or QSDFT for interpretation of the CO_2 adsorption isotherm on zeolites in terms of pore space. Therefore, a new approach based on molecular simulation has been developed to allow the characterization of the zeolite pore space using adsorption isotherms of CO_2. For the specific case of zeolite A samples, the first step was to define a standard CO_2 experimental isotherm. The detailed high-resolution CO_2 isotherms obtained by Palomino et al. [58] (Fig. 5a). at 303 K was chosen for this study.

After that, a force field has been established to reproduce the standard experimental isotherm. The isotherm called SC8 (blue line in Fig. 5a) was simulated using the specified force field, being able to reproduce satisfactorily the experimental isotherm. The force field was set by optimizing the match between simulated and experimental isotherms of the pressure value in the inflection point. With a validated force field, it is possible to reproduce the isotherms under different conditions of pressure and temperature and, more importantly, to verify the influence of each supercage cavity in the experimental isotherms.

The experimental CO_2 adsorption isotherms for the samples synthesized in this study are shown in Fig. 5b. Sample ZA adsorbs 10% more than ZA-MT and ZA-MT/AT samples and 18% more than ZA-AT sample. The IUPAC classification of isotherms is the same for all samples (Type I). The details of the adsorption regime at lower pressures shown in Fig. 5b indicate that all isotherms are consistent with the Si/Al ratio equal to 1 and the decrease in CO_2 adsorption capacity must be related to defects in the supercages. During synthesis, in the stages of nucleation and crystal growth, several classes of defects may be present. These defects are difficult to identify due to the wide variety of chemical species in the mixture and the lack of knowledge of the nature and structure of precursor species. It has been observed that flaws in the structure of zeolite A can be translated as a proportional decrease in the adsorption capacity caused by the non-functionality of a given number of supercage units. Hence, the developed force field has been used to calculate isotherms for a decreasing number of viable supercages. Zeolite A unit cell has 8 supercages viable for adsorption (Fig. 5c).

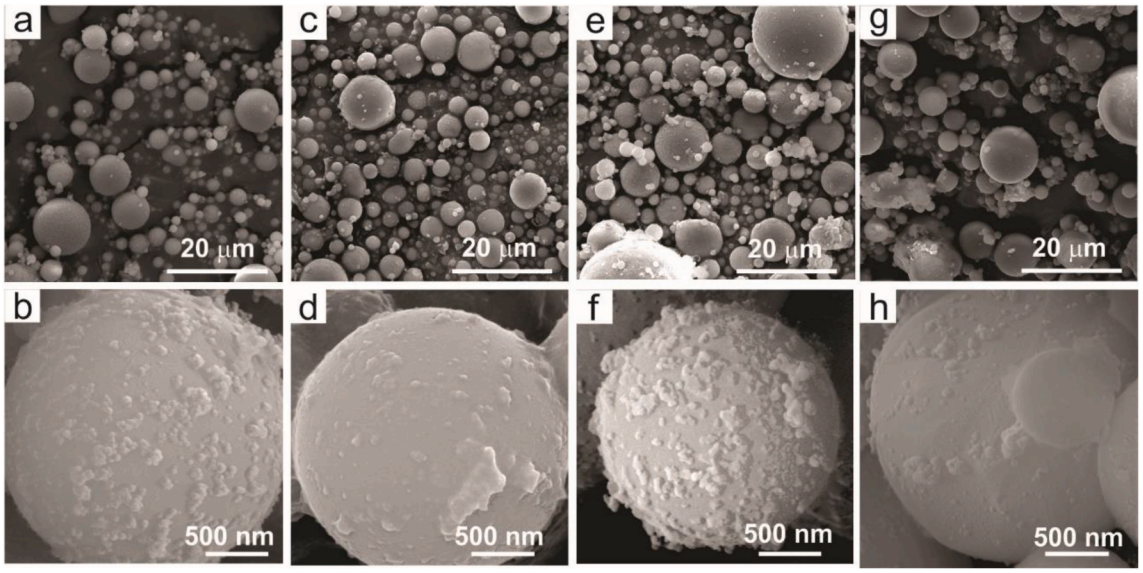

Fig. 3. SEM images of the fly-ash samples (a–b) FA (fly-ash without treatment), and the treated samples (c–d) FA-AT (acid treatment), (e–f) FA-MT (magnetic treatment) and (g–h) FA-MT/AT (combined magnetic and acid treatments).

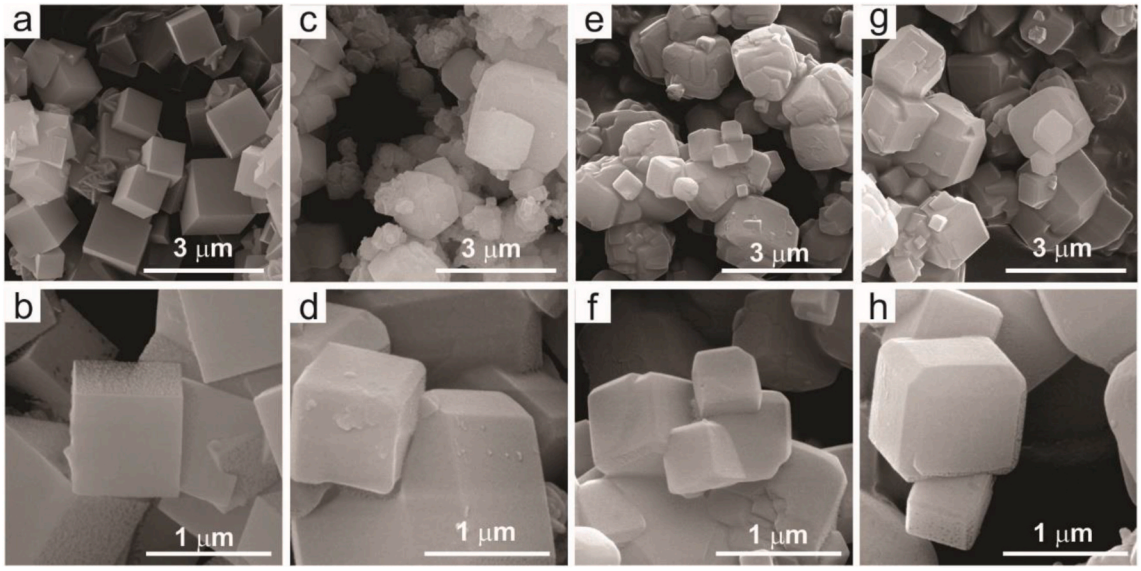

Fig. 4. SEM images of synthesized zeolites (a–b) ZA, (c–d) ZA-AT, (e–f) ZA-MT and (g–h) ZA-MT/AT.

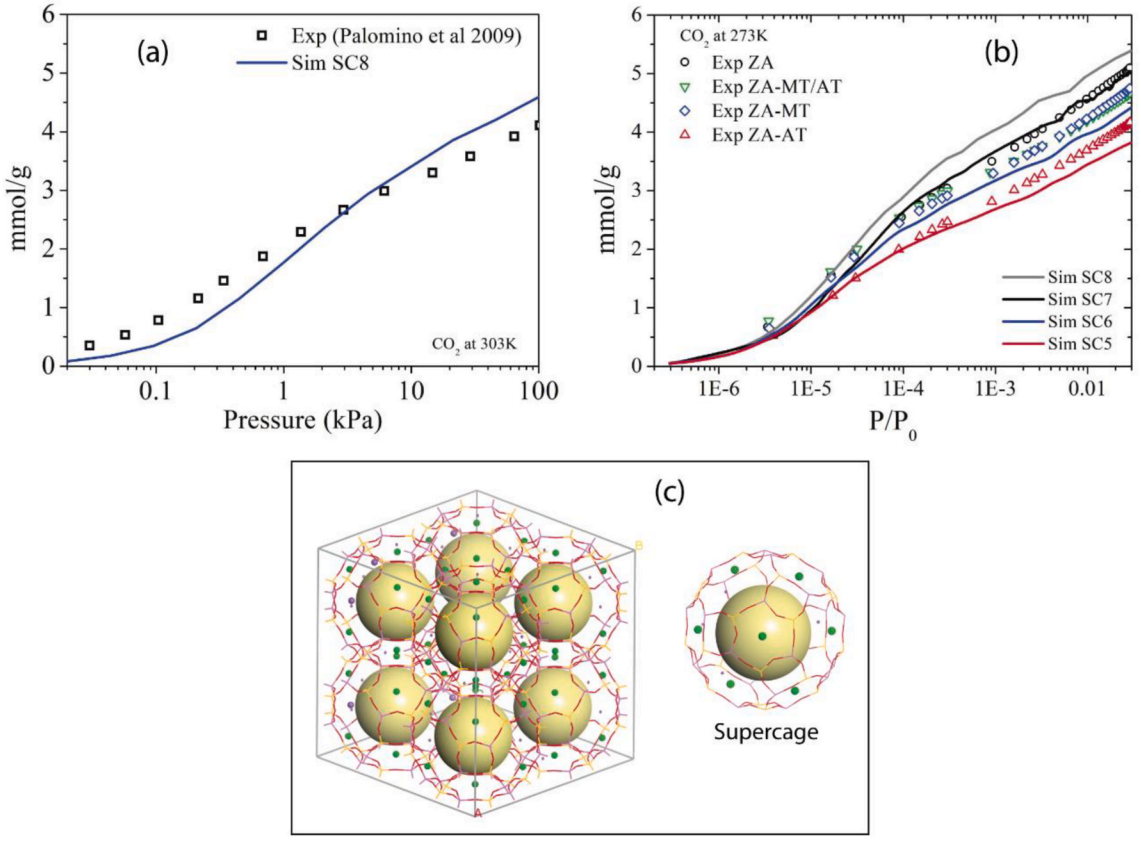

Fig. 5. (a) Standard experimental isotherm (squares) of CO_2 (303 K) for zeolite A and simulated isotherm (line) from the appropriate force field. The SC8 label denotes the number of viable supercages per unit cell (8 supercages/unit cell). (b) Experimental and simulated isotherms of CO_2 for zeolite A at 273 K. Experimental isotherms: ZA (circle), ZA-MT (diamond), ZA-MT/AT (green triangle) and ZA-AT (red triangle). Simulated isotherms: SC8 (gray line), SC7 (black line), SC6 (blue line) and SC6 (red line), the numbers 8, 7, 6 e 5 indicate the viable supercages per unit cell. (c) Framework of a zeolite A unit cell. Each unit cell has 8 supercages. Yellow sphere – pore volume of the supercage. Small spheres – cations. Pink – Al, Yellow – Si and Red – O. (For interpretation of the references to color in this figure legend, the reader is referred to the Web version of this article.)

From the zeolite A structure with all 8 functional supercages, simulations have been made with a decreasing number of functional supercages: 7, 6 and 5 (i.e., inactivation of 1, 2 and 3 supercages per unit cell, respectively). The simulated CO_2 adsorption isotherms are presented in Fig. 5b, together with the experimental data. The gray line (SC8) is the result of the simulated CO_2 adsorption isotherm in a sample without defects, where all supercages are functional. The black (SC7), blue (SC6) and red (SC5) lines are simulated isotherms for theoretical

samples with 7, 6 and 5 viable supercages per unit cell, respectively. The comparison between simulated and experimental isotherms provides interesting conclusions. The ZA sample, with the best performance, appears to have only one defective supercage/unit cell. Considering that an alternative raw material such as fly ash has been used, the synthesis of the ZA sample is an excellent outcome of this study. The structures of ZA-MT and ZA-MT/AT samples are compatible with an average deactivation close to 2 supercages/unit cell and the structure of the worst performing sample, ZA-AT, corresponds to a deactivation of almost 3 supercage/unit cell.

The employed novel characterization approach allows not only the verification of the adsorption capacity of the synthesized samples but also indicates the level of impairment of the porous structure in terms of supercage deactivation.

3.6. Thermal analysis

The role played by zeolite in the warm mix asphalt results from its ability to retain water within its pores and release it at specific temperatures. Thermogravimetric analysis (TGA) and differential scanning calorimetry (DSC) results for zeolite ZA are presented in Fig. 6.

According to the general chemical formula for the unit cell of zeolite A, approximately 22% of its mass corresponds to water. As indicated by TGA, up to 350 °C there is a loss of 17% of mass, which is related to water release. DSC shows distinct thermal events, indicating that water is present in different sites within the zeolite structure. The mass loss around 100 °C refers to adsorbed water, while the loss at higher temperatures (above 200 °C) can be related to dehydration, involving the formation of hydrate complexes with the exchangeable cations [25].

3.7. Rotational viscosity test on the zeolite modified asphalt cement

The result of monitoring the viscosity of AC and ZA-AC samples after heating at 120 °C is presented in Table 4. For AC sample, over the first 60 min the viscosity keeps practically constant, therefore no significant changes are observed.

Compared to the non-modified asphalt cement, the ZA-AC sample (containing zeolite) present a higher viscosity, what is expected as a mineral was used as additive. However, when the ZA-AC sample is heated, a reduction in viscosity is observed within the first 20 min. Such a phenomenon results from the release of water present in the zeolite pores, promoting the micro foaming of the binder and consequently reducing its viscosity and enhancing its workability.

Table 4
Viscosity as a function of time for non-modified asphalt cement (AC) and zeolite modified asphalt cement (ZA-AC), at 120 °C.

Time/min	Absolut viscosity/cP		Percentual viscosity/%	
	ZA-AC	AC	ZA-AC	AC
0.5	887.5	855.0	100	100
1.0	882.5	850.0	99.4	99.7
6.0	865.0	850.0	97.4	99.4
11	860.0	850.0	96.9	99.4
16	860.0	852.5	96.9	99.7
21	857.5	850.0	96.6	99.4
26	852.5	847.5	96.0	99.1
31	852.5	845.0	96.0	98.8

4. Conclusions

In summary, in this paper we have performed a series of different treatments to coal fly ash and applied them to the synthesis of zeolite A, in a high yield process that resulted in a distinguished material. Some aspects of the obtained zeolites showed to be influenced by the type of treatment employed to the fly ash. A novel pore characterization method, based on CO_2 isotherms at 273 K and molecular simulation, revealed that almost all supercages of the synthetized sample ZA are unflawed.

The use of an important industrial by-product for the synthesis of zeolite A with minimum amounts of secondary phases, can dramatically reduce the zeolite production costs, allowing it to be applied in large scale applications such as its use as additive for warm mix asphalt, as demonstrated herein. The performance of the zeolite A, obtained from fly ash, in reducing the viscosity of asphalt cement makes it suitable for this purpose. Hopefully, the double environmental benefit related to the conversion of a waste into a product with high value-added and the considerable energy savings through the viability of WMA processes can drive the adoption of these technologies.

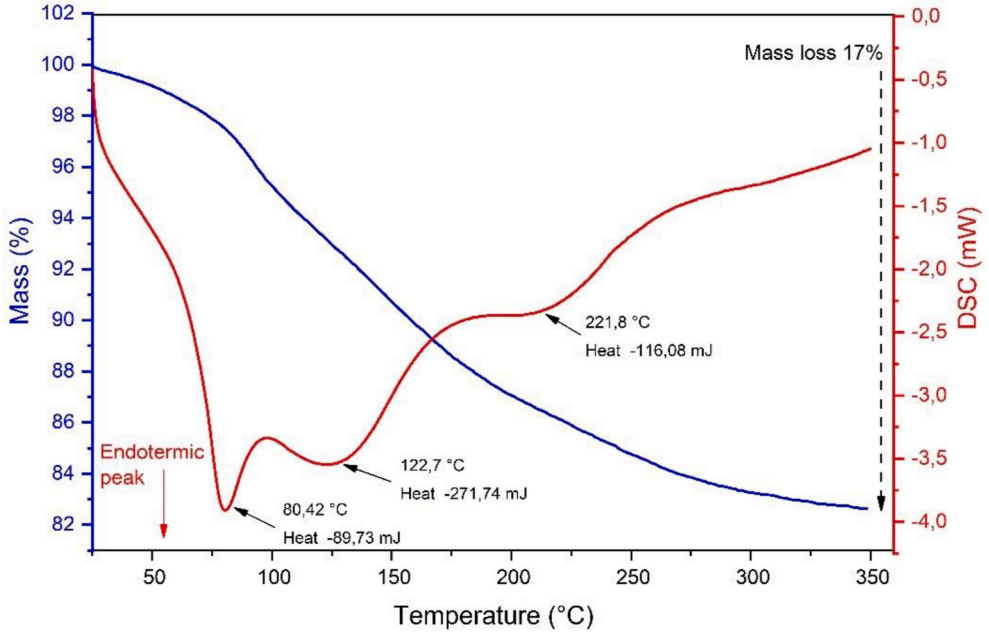

Fig. 6. Thermogravimetric and DSC analysis of sample ZA.

Funding

This study was financed in part by the Coordenação de Aperfeiçoamento de Pessoal de Nível Superior - Brasil (CAPES) - Finance Code 001 (PROEX 23038.000509/2020–82).

CRediT authorship contribution statement

Bruno C. Amoni: Conceptualization, syntheses, Data curation, Formal analysis, Investigation, Writing – original draft, Writing – review & editing. **Armando D.L. Freitas:** Conceptualization, syntheses, Data curation, Formal analysis, Investigation, Writing – original draft, Writing – review & editing. **Raquel A. Bessa:** Syntheses, Data curation, Formal analysis, Investigation, Writing – original draft, Writing – review & editing. **Cristiane P. Oliveira:** Formal analysis, Writing – original draft, Writing – review & editing. **Moisés Bastos-Neto:** CO_2 isotherms acquisition, Data curation, Formal analysis, Investigation, Writing – original draft, Writing – review & editing. **Diana C.S. Azevedo:** CO_2 isotherms acquisition, Data curation, Formal analysis, Investigation, Writing – original draft, Writing – review & editing. **José M. Sasaki:** Data curation, Funding acquisition, Resources, Investigation, Writing – original draft, Writing – review & editing. **Jorge B. Soares:** Conceptualization, Data curation, Funding acquisition, Resources, Investigation, Writing – original draft, Writing – review & editing. **Sandra A. Soares:** Conceptualization, Data curation, Funding acquisition, Resources, Investigation, Writing – original draft, Writing – review & editing. **Adonay R. Loiola:** Conceptualization, Data curation, Funding acquisition, Resources, Supervision, Investigation, Project administration, Writing – original draft, Writing – review & editing.

Declaration of competing interest

The authors declare that they have no known competing financial interests or personal relationships that could have appeared to influence the work reported in this paper.

Acknowledgements

The authors acknowledge ENEVA/EDP group for providing the fly ash, Petrobras/Lubnor for providing the asphalt cement, and Central Analítica of the Federal University of Ceará (UFC/CT-INFRA/MCTI-SISNANO/Pro-Equipamentos CAPES) for the technical support and experiments of scanning electron microscopy.

Appendix A. Supplementary data

Supplementary data to this article can be found online at https://doi.org/10.1016/j.matchemphys.2021.125197.

References

[1] S.S. Bukhari, J. Behin, H. Kazemian, S. Rohani, Conversion of coal fly ash to zeolite utilizing microwave and ultrasound energies: a review, Fuel 140 (2015) 250–266, https://doi.org/10.1016/j.fuel.2014.09.077.
[2] D. Valeev, I. Kunilova, A. Alpatov, A. Mikhailova, M. Goldberg, A. Kondratiev, Complex utilisation of ekibastuz brown coal fly ash: iron & carbon separation and aluminum extraction, J. Clean. Prod. 218 (2019) 192–201, https://doi.org/10.1016/j.jclepro.2019.01.342.
[3] B. Kumar, R. Garg, U. Singh, Utilization of fly ash as filler in HDPE/fly ash polymer composites: a review, Int. J. Appl. Eng. Res. 7 (2012) 1679–1682.
[4] M. Ahmaruzzaman, A review on the utilization of fly ash, Prog. Energy Combust. Sci. 36 (2010) 327–363, https://doi.org/10.1016/j.pecs.2009.11.003.
[5] M. Kaya, M. Uysal, K. Yilmaz, O. Karahan, C.D. Atiş, Mechanical properties of class C and F fly ash geopolymer mortars, Gradevinar 72 (2020) 297–309, https://doi.org/10.14256/JCE.2421.2018.
[6] P. Khoshnoud, S. Gunashekar, M.M. Jamel, N. Abu-Zahra, Comparative analysis of rigid PVC foam reinforced with class C and class F fly ash, J. Miner. Mater. Char. Eng. 2 (2014) 554–565, https://doi.org/10.4236/JMMCE.2014.26057.
[7] R. Dandautiya, A.P. Singh, S. Kundu, Impact assessment of fly ash on ground water quality: an experimental study using batch leaching tests, Waste Manag. Res. 36 (2018) 624–634, https://doi.org/10.1177/0734242X18775484.
[8] P.K. Sharma, J.P. Singh, A. Kumar, Effect of particle size on physical and mechanical properties of fly ash based geopolymers, Trans. Indian Inst. Met. 72 (2019) 1323–1337, https://doi.org/10.1007/s12666-019-01628-w.
[9] Z.T. Yao, X.S. Ji, P.K. Sarker, J.H. Tang, L.Q. Ge, M.S. Xia, Y.Q. Xi, A comprehensive review on the applications of coal fly ash, Earth Sci. Rev. 141 (2015) 105–121, https://doi.org/10.1016/j.earscirev.2014.11.016.
[10] T.F. de Aquino, S.T. Estevam, V.O. Viola, C.R.M. Marques, F.L. Zancan, L. B. Vasconcelos, H.G. Riella, M.J.R. Pires, R. Morales-Ospino, A.E.B. Torres, M. Bastos-Neto, C.L. Cavalcante, CO2 adsorption capacity of zeolites synthesized from coal fly ashes, Fuel 276 (2020) 118143, https://doi.org/10.1016/j.fuel.2020.118143.
[11] Y.P. Chauhan, M. Talib, A novel and green approach of synthesis and characterization of nano-absorbentes (zeolites) from coal fly ash: a review, Sci. Revs. Chem. Commun. 2 (2012) 12–19. www.sadgurupublications.com. (Accessed 16 May 2021). accessed.
[12] J. Weitkamp, Zeolites and catalysis, Solid State Ionics 131 (2000) 175–188, https://doi.org/10.1016/S0167-2738(00)00632-9.
[13] K. Shams, S.J. Mirmohammadi, Preparation of 5A zeolite monolith granular extrudates using kaolin: investigation of the effect of binder on sieving/adsorption properties using a mixture of linear and branched paraffin hydrocarbons, Microporous Mesoporous Mater. 106 (2007) 268–277, https://doi.org/10.1016/j.micromeso.2007.03.007.
[14] C.S. Cundy, P.A. Cox, The hydrothermal synthesis of zeolites: precursors, intermediates and reaction mechanism, Microporous Mesoporous Mater. 82 (2005) 1–78, https://doi.org/10.1016/j.micromeso.2005.02.016.
[15] C.S. Cundy, Microwave techniques in the synthesis and modification of zeolite catalysts. A review, Collect. Czech Chem. Commun. 63 (1998) 1699–1723, https://doi.org/10.1135/cccc19981699.
[16] S. Askari, S. Miar Alipour, R. Halladj, M.H. Davood Abadi Farahani, Effects of ultrasound on the synthesis of zeolites: a review, J. Porous Mater. 20 (2013) 285–302, https://doi.org/10.1007/s10934-012-9598-6.
[17] R.A. Bessa, L.S. Costa, C.P. Oliveira, F. Bohn, R.F. Nascimento, J.M. Sasaki, A. R. Loiola, Kaolin-based magnetic zeolites A and P as water softeners, Microporous Mesoporous Mater. 245 (2017) 64–72, https://doi.org/10.1016/j.micromeso.2017.03.004.
[18] M. Visa, Synthesis and characterization of new zeolite materials obtained from fly ash for heavy metals removal in advanced wastewater treatment, Powder Technol. 294 (2016) 338–347, https://doi.org/10.1016/j.powtec.2016.02.019.
[19] T. Yang, C. Han, H. Liu, L. Yang, D. Liu, J. Tang, Y. Luo, Synthesis of Na-X zeolite from low aluminum coal fly ash: characterization and high efficient As(V) removal, Adv. Powder Technol. 30 (2019) 199–206, https://doi.org/10.1016/J.APT.2018.10.023.
[20] H. Holler, U. Wirsching, Zeolite formation from fly ash, Fortschr. Mineral. 63 (1985) 21–43.
[21] H. Deng, Y. Ge, Formation of NaP zeolite from fused fly ash for the removal of Cu (II) by an improved hydrothermal method, RSC Adv. 5 (2015) 9180–9188, https://doi.org/10.1039/c4ra15196h.
[22] K.S. Hui, C.Y.H. Chao, Effects of step-change of synthesis temperature on synthesis of zeolite 4A from coal fly ash, Microporous Mesoporous Mater. 88 (2006) 145–151, https://doi.org/10.1016/j.micromeso.2005.09.005.
[23] J. Behin, S.S. Bukhari, V. Dehnavi, H. Kazemian, S. Rohani, Using coal fly ash and wastewater for microwave synthesis of LTA zeolite, Chem. Eng. Technol. 37 (2014) 1532–1540, https://doi.org/10.1002/ceat.201400225.
[24] J.D.C. Izidoro, D.A. Fungaro, F.S. Dos Santos, S. Wang, Characteristics of Brazilian coal fly ashes and their synthesized zeolites, Fuel Process. Technol. 97 (2012) 38–44, https://doi.org/10.1016/j.fuproc.2012.01.009.
[25] S. Goñi, R. Peña, A. Guerrero, Hydrothermal synthesis of zeolite from coal class F fly ash. Influence of temperature, Mater. Construcción 60 (2010) 51–60, https://doi.org/10.3989/mc.2010.47808.
[26] N.M. Musyoka, L.F. Petrik, E. Hums, A. Kuhnt, W. Schwieger, Thermal stability studies of zeolites A and X synthesized from South African coal fly ash, Res. Chem. Intermed. 41 (2015) 575–582, https://doi.org/10.1007/s11164-013-1211-3.
[27] N.M. Musyoka, L.F. Petrik, E. Hums, H. Baser, W. Schwieger, In situ ultrasonic diagnostic of zeolite X crystallization with novel (hierarchical) morphology from coal fly ash, Ultrasonics 54 (2014) 537–543, https://doi.org/10.1016/j.ultras.2013.08.005.
[28] A.M. Cardoso, M.B. Horn, L.S. Ferret, C.M.N. Azevedo, M. Pires, Integrated synthesis of zeolites 4A and Na-P1 using coal fly ash for application in the formulation of detergents and swine wastewater treatment, J. Hazard Mater. 287 (2015) 69–77, https://doi.org/10.1016/j.jhazmat.2015.01.042.
[29] A. Topal, B. Sengoz, B.V. Kok, M. Yilmaz, P.A. Dokandari, J. Oner, D. Kaya, Evaluation of mixture characteristics of warm mix asphalt involving natural and synthetic zeolite additives, Construct. Build. Mater. 57 (2014) 38–44, https://doi.org/10.1016/j.conbuildmat.2014.01.093.
[30] ASTM, C618-19, Standard Specification for Coal Fly Ash and Raw or Calcined Natural Pozzolan for Use in Concrete, ASTM Int. Conshohocken, 2019. https://www.astm.org/Standards/C618.
[31] A.C. Larson, R.B. Von, D. Lansce, General Structure Analysis System (GSAS), Los Alamos Natl. Lab. Rep. LAUR 86-748, Los Alamos, USA, 2004.
[32] B.H. Toby, EXPGUI, a graphical user interface for GSAS, J. Appl. Crystallogr. 34 (2001) 210–213, https://doi.org/10.1107/S0021889801002242.

[33] P. Scherrer, Bestimmung der inneren Struktur und der Größe von Kolloidteilchen mittels Röntgenstrahlen, Kolloidchem. Ein Lehrb (1912) 387–409, https://doi.org/10.1007/978-3-662-33915-2_7.
[34] J.J. Pluth, J.V. Smith, Accurate redetermination of crystal structure of dehydrated zeolite A. Absence of near zero coordination of sodium. Refinement of Si,Al-ordered superstructure, J. Am. Chem. Soc. 102 (1980) 4704–4708, https://doi.org/10.1021/ja00534a024.
[35] J.G. Harris, K.H. Yung, Carbon dioxide's liquid-vapor coexistence curve and critical properties as predicted by a simple molecular model, J. Phys. Chem. 99 (1995) 12021–12024, https://doi.org/10.1021/j100031a034.
[36] V.A.M. Gomes, J.A. Coelho, H.R. Peixoto, S.M.P. Lucena, Easily tunable parameterization of a force field for gas adsorption on FAU zeolites, Adsorption 21 (2015) 25–35, https://doi.org/10.1007/s10450-014-9647-3.
[37] B.C. Amoni, Development of a Method for Synthesis of Zeolite Type A Using Coal Fly Ash: Evaluation of its Use as a Warm Asphalt Mixture Additive, Doctoral Thesis, Federal University of Ceará, Fortaleza, Ceará, 2019.
[38] A. Woszuk, W. Franus, Properties of the Warm Mix Asphalt involving clinoptilolite and Na-P1 zeolite additives, Construct. Build. Mater. 114 (2016) 556–563, https://doi.org/10.1016/J.CONBUILDMAT.2016.03.188.
[39] G.C. Hurley, B.D. Prowell, NCAT report 05-06 - evaluation of sasobit for use in warm mix asphalt, NCAT Rep. 5–6 (2005) 32. https://citeseerx.ist.psu.edu/viewdoc/download?doi=10.1.1.484.7388&rep=rep1&type=pdf. (Accessed 9 July 2021). accessed.
[40] Ó. Kristjánsdottir, S.T. Muench, L. Michael, G. Burke, Assessing potential for warm-mix asphalt technology adoption, Transport. Res. Rec. (2007) 91–99, https://doi.org/10.3141/2040-10.
[41] M. Mazumder, H. Kim, S.J. Lee, Performance properties of polymer modified asphalt binders containing wax additives, Int. J. Pavement Res. Technol. 9 (2016) 128–139, https://doi.org/10.1016/J.IJPRT.2016.03.004.
[42] V. Gramlich, W.M. Meier, The crystal structure of hydrated NaA : a detailed refinement of a pseudosymmetric zeolite structure, Z. für Kristallogr. - Cryst. Mater. 133 (1971) 134–149, https://doi.org/10.1524/ZKRI.1971.133.16.134.
[43] J.A. Van Bokhoven, T.L. Lee, M. Drakopoulos, C. Lamberti, S. Thie, J. Zegenhagen, Determining the aluminium occupancy on the active T-sites in zeolites using X-ray standing waves, Nat. Mater. 7 (2008) 551–555, https://doi.org/10.1038/nmat2220.
[44] S.S. Bukhari, J. Behin, H. Kazemian, S. Rohani, A comparative study using direct hydrothermal and indirect fusion methods to produce zeolites from coal fly ash utilizing single-mode microwave energy, 2014, J. Mater. Sci. 49 (2014) 8261–8271, https://doi.org/10.1007/S10853-014-8535-2, 4924.
[45] Y. Yaping, Z. Xiaoqiang, Q. Weilan, W. Mingwen, Synthesis of pure zeolites from supersaturated silicon and aluminum alkali extracts from fused coal fly ash, Fuel 87 (2008) 1880–1886, https://doi.org/10.1016/J.FUEL.2007.12.002.
[46] Y. Watanabe, H. Yamada, J. Tanaka, Y. Komatsu, Y. Moriyoshi, Ammonium ion exchange of synthetic zeolites: the effect of their open-window sizes, pore structures, and cation exchange capacities, Separ. Sci. Technol. 39 (2004) 2091–2104, https://doi.org/10.1081/SS-120039306.
[47] W. Mozgawa, M. Król, J. Dyczek, J. Deja, Investigation of the coal fly ashes using IR spectroscopy, Spectrochim. Acta Part A Mol. Biomol. Spectrosc. 132 (2014) 889–894, https://doi.org/10.1016/j.saa.2014.05.052.
[48] Y. Huang, Z. Jiang, Vibrational spectra of completely siliceous zeolite A, Microporous Mater. 12 (1997) 341–345, https://doi.org/10.1016/S0927-6513(97)00082-5.
[49] A.R. Loiola, J.C.R.A. Andrade, J.M. Sasaki, L.R.D. da Silva, Structural analysis of zeolite NaA synthesized by a cost-effective hydrothermal method using kaolin and its use as water softener, J. Colloid Interface Sci. 367 (2012) 34–39, https://doi.org/10.1016/j.jcis.2010.11.026.
[50] D.H. Vu, H.B. Bui, B. Kalantar, X.N. Bui, D.A. Nguyen, Q.T. Le, N.H. Do, H. Nguyen, Composition and morphology characteristics of magnetic fractions of coal fly ash wastes processed in high-temperature exposure in thermal power plants, Appl. Sci. 9 (2019) 1964, https://doi.org/10.3390/app9091964.
[51] A. Bourliva, L. Papadopoulou, E. Aidona, K. Simeonidis, G. Vourlias, E. Devlin, Y. Sanakis, Enrichment and oral bioaccessibility of selected trace elements in fly ash-derived magnetic components, Environ. Sci. Pollut. Res. 24 (2017) 2337–2349, https://doi.org/10.1007/s11356-016-7967-4.
[52] W. Greń, S.C. Parker, B. Slater, D.W. Lewis, Structure of zeolite A (LTA) surfaces and the zeolite A/water interface, J. Phys. Chem. C 114 (2010) 9739–9747, https://doi.org/10.1021/jp909355e.
[53] B. Jensen, B. Kvamme, T. Kuznetsova, The effect of interfacial charge distributions and terminations in LTA zeolites, Microporous Mesoporous Mater. 224 (2016) 135–142, https://doi.org/10.1016/j.micromeso.2015.11.031.
[54] J. Bronić, A. Palčić, B. Subotić, L. Itani, V. Valtchev, Influence of alkalinity of the starting system on size and morphology of the zeolite A crystals, Mater. Chem. Phys. 132 (2012) 973–976, https://doi.org/10.1016/j.matchemphys.2011.12.043.
[55] C.I. Round, S.J. Hill, K. Latham, C.D. Williams, The crystal morphology of zeolite A. The effects of the source of the reagents, Microporous Mater. 11 (1997) 213–225, https://doi.org/10.1016/S0927-6513(97)00051-5.
[56] F. Rouquerol, J. Rouquerol, K. Sing, Adsorption by clays, pillared layer structures and zeolites, in: Adsorpt. By Powders Porous Solids, Elsevier, 1999, pp. 355–399, https://doi.org/10.1016/b978-012598920-6/50012-9.
[57] K.C. Kim, T.U. Yoon, Y.S. Bae, Applicability of using CO2 adsorption isotherms to determine BET surface areas of microporous materials, Microporous Mesoporous Mater. 224 (2016) 294–301, https://doi.org/10.1016/j.micromeso.2016.01.003.
[58] M. Palomino, A. Corma, F. Rey, S. Valencia, New insights on C02-methane separation using LTA zeolites with different Si/Al ratios and a first comparison with MOFs, Langmuir 26 (2010) 1910–1917, https://doi.org/10.1021/la9026656.